Available online at www.sciencedirect.com
ScienceDirect
Acta Materialia 58 (2010) 5274–5285
Acta MATERIALIA
www.elsevier.com/locate/actamat

Recent developments in the study of hydrogen embrittlement: Hydrogen effect on dislocation nucleation

Afrooz Barnoush *, Horst Vehoff

Saarland University, Department of Materials Science, Bldg. D22, P.O. Box 151150, D-66041 Saarbruecken, Germany

Received 11 March 2010; received in revised form 30 May 2010; accepted 30 May 2010
Available online 2 July 2010

Abstract

In this paper, the intrinsic complexities of the experimental examination of hydrogen embrittlement are discussed. On the basis of these complexities, an experimental approach, in situ electrochemical nanoindentation, is proposed and performed on different materials. This technique is capable of registering the onset of plasticity in extremely small volumes, namely perfect crystals in hydrogen-free and charged conditions. It is shown that hydrogen reduces the required stress for the onset of plasticity, i.e. homogeneous dislocation nucleation by reduction in the shear modulus, dislocation line energy and stacking fault energy. The change in the shear modulus can be related to reduction in crystal cohesion whereas the reduction in dislocation line energy and stacking fault energy are explained by the defactant concept, i.e. reduction in the defect formation energy in the presence of hydrogen. Thus, neither hydrogen-enhanced decohesion nor hydrogen-enhanced plasticity, but the reduction in the cohesion and defect formation energy are responsible for hydrogen embrittlement.

Keywords: Hydrogen embrittlement; Nanoindentation; Yield phenomena; Electrochemistry; Dislocation nucleation

1. Introduction

Hydrogen embrittlement is a severe environmental type of failure that affects almost all metals and alloys. With advancing technology, the use of high-strength structural materials for lightweight construction and energy conservation becomes a necessity. In spite of the success of materials scientists in developing alloys with outstanding combinations of high tensile strength and high fracture toughness, hydrogen embrittlement still has a widespread effect that severely degrades the fracture resistance of these alloys. On the other hand, with the depletion of fossil fuels, mankind is searching for other sources of energy. Hydrogen is believed to be a possible future energy source and it is very possible that a "hydrogen economy" will be realized within the next 50 years. In such a scenario, large-scale production, storage, transportation and use of hydrogen will become necessary. However, the problems in materials caused by hydrogen embrittlement, reported as early as 1875 by Johnson [1], could limit the progress of such an economy. Since Johnson first reported on hydrogen embrittlement, various strong views on the mechanisms of hydrogen embrittlement have been vigorously discussed and thoroughly reviewed in the literature [2–4]. Because of the technological importance of hydrogen embrittlement, many people have explored the nature, causes and control of hydrogen-related degradation of metals [5–7]. This has resulted in an enormous number of sometimes controversial findings and/or interpretations. Moreover, frequently an ad hoc approach, focusing on urgent technical problems at hand, is adopted which raises the question of how this isolated case or interpretation really reflects on any basic, general concepts. It thus seems apparent that the findings gathered so far cannot be accounted for by a single dominant mechanism.

As an example, Fig. 1 shows the results of conventional hydrogen embrittlement testing of 34 different grades of

* Corresponding author.
E-mail address: a.barnoush@matsci.uni-sb.de (A. Barnoush).

1359-6454/$36.00 © 2010 Acta Materialia Inc. Published by Elsevier Ltd. All rights reserved.
doi:10.1016/j.actamat.2010.05.057

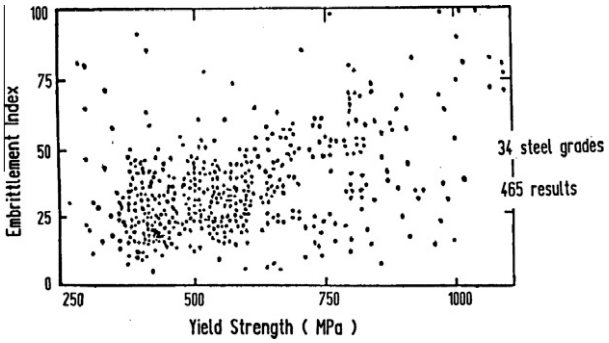

Fig. 1. The hydrogen embrittlement index measured by conventional mechanical testing for 34 different grades of steel within 465 test runs [8].

steel within 465 test runs [8]. The embrittlement index shown in Fig. 1 is the reduction in the fracture area in hydrogen-charged vs. hydrogen-free conditions during uniaxial tensile tests. The scatter observed within the results shown in Fig. 1 demonstrates the need for a new experimental approach to the investigation of hydrogen embrittlement. It is necessary to find the source of this scatter in conventional hydrogen embrittlement testing methods. In this paper we will briefly review the different experimental approaches used to study hydrogen embrittlement with a special focus on in situ local examination methods of hydrogen–dislocation interactions due to the conclusive role of dislocations in fracture and hydrogen embrittlement of metals. Then we will discuss the recently developed in situ electrochemical nanoindentation (ECNI) technique and its advantages in the study of hydrogen embrittlement.

2. Experimental approach to hydrogen embrittlement

Hydrogen–deformation interactions have many facets with broad implications. These can be divided into three main aspects, as shown in Fig. 2. Numerous systems and circumstances in terms of environmental or even purely mechanical aspects are only part of the issue. An additional aspect is the wide range of intrinsic/extrinsic variables concerning the material itself. The experimental approach for examination of hydrogen embrittlement is based on the elimination of diverse factors within these three aspects. For example, let us consider uniaxial straining of a single crystal sample combined with controlled hydrogen charging on the surface. The uniaxial stress field simplifies the stress condition, i.e. the mechanical aspect of hydrogen embrittlement, in the test. Use of a single crystal and controlled hydrogen charging condition reduces the complexities due to the material and environmental aspects of hydrogen embrittlement in the test. Unfortunately, due to the large difference in the scale of these aspects controlling the process of hydrogen embrittlement, this experimental methodology is not very successful. The uniaxial stress field of the above-mentioned example is not uniform, unlike the scale of hydrogen interacting with defects like dislocations and vacancies. This problem becomes more complicated as the microstructure becomes more complex with the introduction of grain boundaries, pores, second phases, etc. On the other hand, surface hydrogen charging of macroscopic samples results in a concentration gradient, which again can override the microscopic process of hydrogen embrittlement. Additionally, microstructural features like dislocations, grain boundaries and interfaces can interact with hydrogen diffusion by providing faster diffusion routes or acting as traps for hydrogen. Superimpose upon this the relative strength of each interface in the presence and absence of hydrogen and the prediction of initiation sites becomes problematic. Finally, since initiation may favor grain boundary failure in one instance and precipitate shearing in another, either boundary decohesion or shear decohesion as enhanced by localized plasticity may result. Either outcome can be favored by simply changing the external state of stress, yield strength level or thermal history. It also becomes apparent that, depending on the experimental approach, one might conclude that a given material is failing due to enhanced cleavage, enhanced

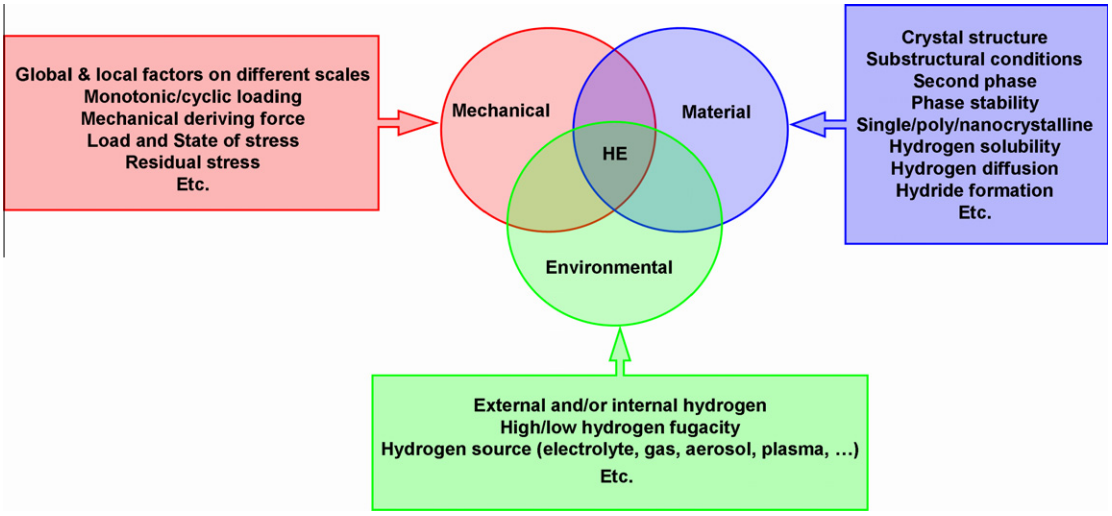

Fig. 2. Global description of hydrogen embrittlement interaction aspects.

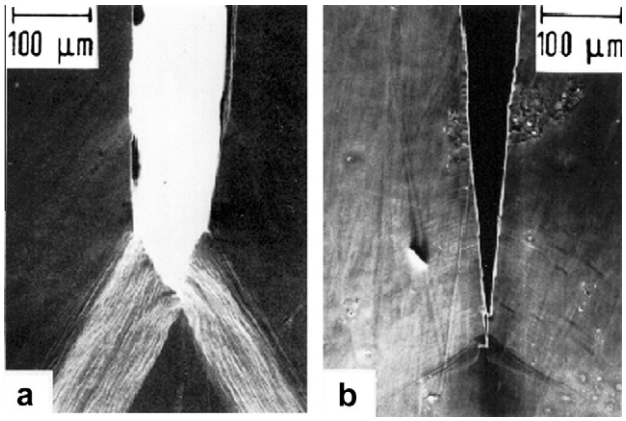

Fig. 3. Hydrogen effect on the crack tip opening angle in: (a) vacuum and (b) hydrogen atmosphere. Sharpness of the crack tip in stressed Fe–3 wt.% Si single crystal increases progressively with increasing hydrogen pressure [10].

grain boundary fracture, enhanced shear or enhanced localized microvoid formation, or all of the above.

One possible solution to these problems, arising from the experimental methodology used for studying hydrogen embrittlement, is the local examination of the hydrogen effect. This entails reducing the scale of the testing method down to the microstructural level such that all three controlling aspects of hydrogen embrittlement (Fig. 2) can be defined within the test. Few attempts of this kind of approach have been done previously. Vehoff and Neumann [9] developed a method for studying crack propagation in a controlled environment under controlled plastic strain conditions. This method was used to study the hydrogen effect on crack growth mechanisms in Fe–2.6% Si [10] and Ni [11]. In their experiments they controlled: (i) environmental aspects by using an ultrahigh-vacuum chamber and controlling the partial pressure of hydrogen; (2) mechanical aspects by controlling plastic strain and confining the stress to a small field ahead of the crack; and (iii) material aspects by selection of specifically oriented single crystals and focusing on the fracture process zone (Fig. 3). Through these perfectly defined experimental conditions they were able to propose a model based on hydrogen-enhanced decohesion (HEDE) and hydrogen trapping in front of a crack tip in the fracture process zone [10,11].

Another intelligent experimental approach for small-scale observation of hydrogen effects on mechanical properties was use of in situ straining tests in an environmental transmission electron microscope (TEM) developed by Birnbaum and Sofronis [12]. With this technique it was possible for the first time to directly observe the effect of hydrogen on dislocations. Unfortunately, there are some uncertainties within the experimental conditions of this technique which must be mentioned here: (i) The electron beam dissociates hydrogen molecules to produce atomic hydrogen. Bond et al. [13] determined that the fugacity of the dissociated hydrogen was between 30 and 750 MPa. (ii) Since mode III (shear off) is usually easier in thin films, crack growth experiments under a defined mode I loading are very difficult to realize and therefore interpretation of the crack growth results become very difficult. (iii) Field of view is limited to the transparent region of the sample.

By the introduction of micro- and nanoscale mechanical testing methods, like instrumented nanoindentation (NI) and nanoindenting atomic force microscopy (NI-AFM), a new era in mechanical testing of extremely small volumes started [14]. Gerberich et al. [15] was the first one who mentioned the potential application of micromechanical tests for the examination of hydrogen embrittlement. Since then, several researchers have used the NI technique to probe the effects of hydrogen on mechanical properties [16–20]. The main advantage of the NI technique is its capability to resolve the dislocation nucleation in samples with low dislocation density [21,22]. Additionally, analytical solutions for stress underneath the tip prior to dislocation nucleation within the elastic deformation are available, so the mechanical aspects of the experiments can be defined. The volume probed during the test is extremely small and can be characterized by means of different techniques, like electron backscatter diffraction (EBSD) and electron channeling contrast [23], and therefore, material aspects can be resolved. The referenced studies [16–20] used ex situ hydrogen charging techniques which resulted in uncertainties

Table 1
Summary of the high-resolution testing methods used for local examination of hydrogen embrittlement.

Experimental approach	Different aspects of the hydrogen embrittlement		
	Mechanical	Environmental	Material
In situ crack propagation test	Defined and analytically can be treated	Defined	Defined in the case of macroscopic single crystals with specific orientation, very hard to apply on complex microstructures
In situ environmental TEM tests	Undefined	Undefined due to dissociation of H molecules by electron beam (low pressure, very high fugacity)	Defined with very high-resolution but only within the field of view
Nanoindentation on ex situ charged samples	Before pop-in is defined and can analytically be treated	Undefined, due to out gassing and concentration gradient	Perfect defect-free crystal
In situ EC nanoindentation	Before pop-in is defined and can analytically be treated	Defined	Perfect defect-free crystal

within the hydrogen concentration especially near the surface of the sample where the mechanical testing was carried out. We solved this problem by performing in situ ECNI tests while the surface hydrogen concentration was kept constant by setting the surface electrochemical potential inside the proper electrolyte [24–26].

Table 1 summarizes the local high-resolution techniques for examination of hydrogen embrittlement. A comparison of these methods shows the advantage of ECNI in providing the required conditions to perform a defined experiment in accordance with different aspects of hydrogen embrittlement. In this paper, we report the results of ECNI tests on different metals with different hydrogen embrittlement susceptibilities. It will be shown that ECNI is capable of quantitatively resolving the sensitivity to hydrogen embrittlement.

3. Experimental

3.1. Materials

The materials used in this study and the electropolishing parameters and electrochemical hydrogen charging conditions for each are summarized in Tables 2 and 3. The single-crystal specimens were cut by spark erosion from large single crystals with a misalignment of less than 2° controlled by EBSD. The polycrystalline specimens were cut from samples with large grains a few millimeters in diameter which act like a single crystal during NI when all tests are performed in the same grain. Large grains or single crystals eliminate the scatter in the data due to orientation differences. The samples were mechanically polished down to 0.25 μm. Afterwards, samples were annealed at 80% of the melting temperature in a vacuum greater than 10^{-6} mbar for 24 h and cooled in the furnace in order to minimize the lattice defect density. Immediately before indentation the samples were electropolished according to the parameters given in Table 2 to have a well-defined reproducible surface condition. Special attention was paid to surface preparation since, as mentioned before, a defect-free and low-roughness surface is necessary in order to observe the dislocation nucleation during NI. When examined with an AFM, the sample surface had an root-mean-square roughness of less than 1 nm, and asperities or steps appeared infrequently on the surface.

3.2. Instrumentation

The experiments were performed with a Hysitron TriboScope® in conjunction with a Digital Instruments Nanoscope II® and a Hysitron TriboIndenter®. The indenter, designed especially for tests in liquid, had a Berkovich or conical diamond tip (see Table 3). For the NI-AFM system, a three-electrode electrochemical setup with a platinum counter electrode and an Ag/AgCl reference electrode was developed, as shown schematically in Fig. 4. Consequently, all the electrochemical potentials in this work are reported against an Ag/AgCl reference electrode. A Bank Elektronik TG 97 potentiostat was used to control the electrochemical potentials, and the electrochemical data were recorded on a PC using an AD–DA interface. The cell was made from Teflon™, and made to fit into the nanoindenter sample holder. Nanoindentation tests were made inside this electrochemical cell while the sample was covered with approximately 2 mm of electrolyte. The whole system was put into a chamber containing a protective atmosphere of nitrogen and helium in order to eliminate the oxygen effect in the electrochemical reaction. The solution was injected from outside the chamber through a polyethylene tube connected to a MicroFil™ pipette.

There are additional concerns that arise when indenting in a liquid environment due to the capillary and buoyancy

Table 2
Summary of the samples studied and their electropolishing conditions.

Material	Purity	Microstructure	Electropolishing condition			
			Solution	Potential (V)	Temperature (°C)	Time (s)
Copper	Zone refined	(1 1 1)	H_3PO_4/ethanol	20	20	30
Aluminum	99.99	1 mm grains	$HClO_4$/ethanol	40	0	30
Fe–3 wt.% Si	See Table 4	1 mm grains	H_2SO_4/CH_3OH	12	10	60
FeAl (40 at.% Al)	Zone refined	(1 0 0)	H_2SO_4/CH_3OH	35	10	90
Nickel	Zone refined	(1 1 1)	H_2SO_4/CH_3OH	30	15	60

Table 3
Summary of the electrochemical hydrogen charging and discharging (passivation) conditions.

Material	Test solution	pH	H-charging potential	Passivation potential	Indenter tip
Copper	Borate buffer	9	−1000 mV	250 mV	Berkovich
Aluminum	Borate buffer	9	−1250 mV	OCP	Berkovich
Aluminum	0.05 M Na_2SO_4	6	OCP	250 mV	Berkovich
Fe–3 wt.% Si	Borate buffer	9	−1000 mV	n.a.	Berkovich
FeAl	0.05 M Na_2SO_4	6	−1100 mV	100 mV	Conical
Nickel	0.05 M Na_2SO_4	6	−1000 mV	500 mV	Berkovich

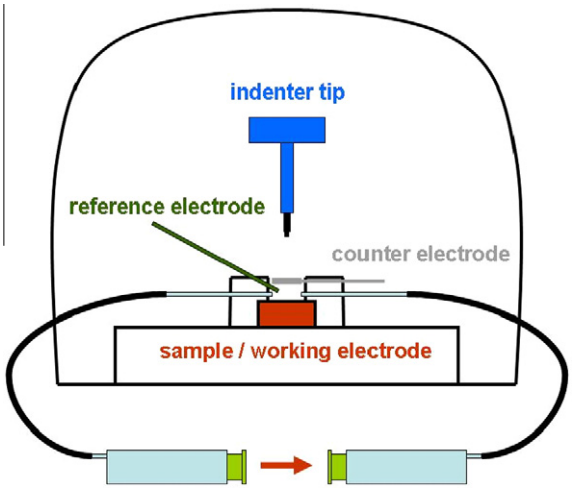

Fig. 4. Schematic drawing of the experimental setup.

forces acting on the tip. To overcome this, the surface is first engaged with a higher set point of contact force. The tip is then moved a few nanometres away from the surface and the forces on the tip balance while it rests above the surface. After this procedure the surface can be easily engaged as usual. Another important concern during the in situ ECNI test is cleanliness. Therefore, all electrolytes were prepared from analytical grade compounds and double-distilled water. Prior to the tests, the electrochemical cell was cleaned in piranha acid to remove most organic matter and to make it hydrophilic and water compatible. The tip and its shaft were also cleaned carefully before each test in a mixture of ethanol and isopropanol and then in double-distilled water. A clean tip shaft reduces the capillary forces acting on it and reduces the probability of disengagement of the tip during surface imaging inside the solution. A low impurity content in the electrolyte inhibits the deposition of these impurities during electrochemical polarization of the surface. The electrolyte pH and composition should also be selected very carefully to inhibit any possible corrosion and surface roughening. Hence, these parameters are selected for each sample individually.

4. Results

4.1. Copper

Copper is known for its very low hydrogen solubility and diffusivity. DeWulf and Bard [27] showed that without hydrogen recombination poisons (e.g. As_2O_3) no detectable hydrogen concentration develops in copper. This makes the copper a proper calibration material for in situ ECNI tests, where no effect of cathodic charging should be observed. Typical load–displacement (L–D) curves under cathodic and anodic potentials are given in Fig. 5.

4.2. Aluminum

Aluminum is a reactive metal protected by a thin stable oxide layer with semi-conductive properties. At potentials cathodic to the open circuit potential (OCP) of Al, cathodic hydrogen evolution due to the reduction of hydrogen ions and water occurs simultaneously with anodic oxidation and dissolution processes [28]. This makes the electrochemical hydrogen charging of Al without damaging the surface difficult. Therefore, an alternative method controlling the pH of the solution was developed and used for hydrogen charging of Al [29]. It is well known that oxide-covered metals immersed in aqueous solutions terminate in an outermost layer of hydroxyl groups due to their interaction with water molecules [30]. In aqueous solutions, the surface hydroxyl groups will remain undissociated if the pH of the

Table 4
Analysis of the Fe–3 wt.% Si alloy used in this study in.

C	Si	Mn	P	S	Cr	Ni	Mo	Cu	Al	Ti	Nb	V	B	Zr	Ce
0.003	2.383	0.202	0.013	0.012	0.033	0.048	0.015	0.020	0.365	0.005	0.020	0.002	0.0008	0.005	0.009

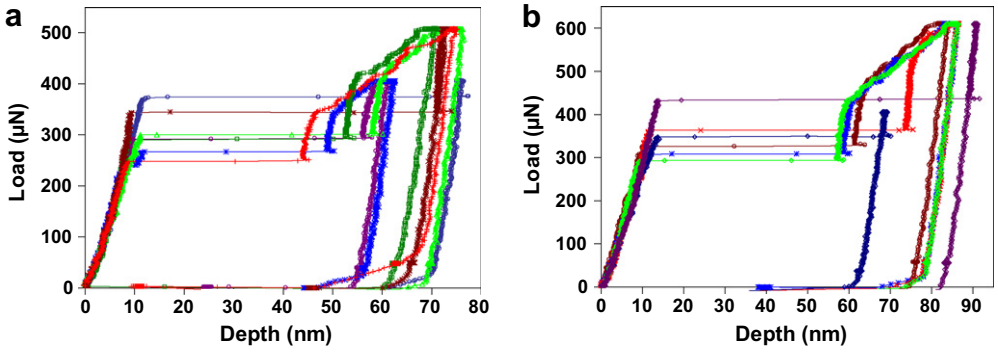

Fig. 5. Typical L–D curves of copper under: (a) cathodic and (b) anodic polarization.

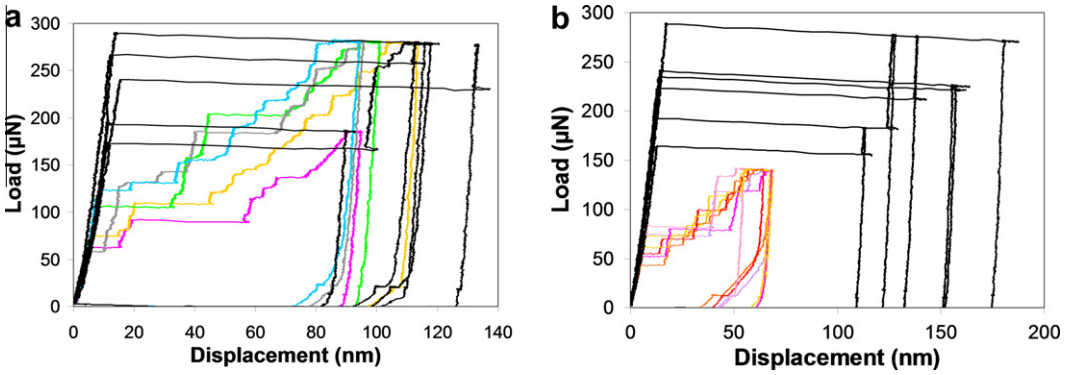

Fig. 6. Typical *L–D* curves of aluminum in: (a) pH6 solution (OCP light-colored/anodic dark-colored) and (b) pH9 solution (cathodic light-colored/OCP dark-colored).

aqueous solution is the same as the isoelectric point (IEP) of the oxide. If the pH is less than the IEP, the surface will acquire a positive charge.

$$MOH_{(surf)} + H^{+}_{(aq)} \rightarrow MOH^{+}_{2(surf)} \quad (1)$$

If the pH is greater than the IEP, the surface will acquire a negative charge

$$MOH_{(surf)} + OH^{-}_{(aq)} \rightarrow MO^{-}_{(surf)} + H_2O \quad (2)$$

The air-formed oxide film on Al has the IEP value of 9.5 [31]. According to the Eqs. (1) and (2), the pH can greatly affect the hydrogen absorption during immersion of the sample in electrolyte under OCP. Hence, the tests on Al were performed in two different solutions (Table 3). Typical *L–D* curves of the aluminum sample at different pH levels and electrochemical polarizations are given in Fig. 6.

4.3. Fe–3 wt.% Si

The Fe–3 wt.% Si alloy is a single-phase body-centered cubic crystal. The electrochemical behavior of this metal is quite similar to that of pure iron and has a very low aqueous corrosion resistance in solutions with low pH. Therefore, in situ ECNI tests were performed in a pH 9 borate buffer solution. This electrolyte is preferred because of the possibility of both controlled cathodic removal of prior oxide films and highly efficient anodic passivation. However, during the in situ ECNI experiments, due to the limited volume of the electrochemical cell and the use of Ag/AgCl reference electrodes, contamination of electrolyte with Cl^{-} ions resulted in the breakdown of the passive layer. All attempts for producing a stable passive layer failed and resulted in a corroded surface that was not suitable for NI experiments. Therefore, in the case of the Fe–3 wt.% Si sample, the NI results under cathodic potential are compared with the results in air. Fig. 7a shows typical load displacement curves during NI of the Fe–3 wt.% Si sample in air. The same sample was indented in the same grain under a cathodic potential of −1000 mV. This resulted in the load displacement curves shown in Fig. 7b.

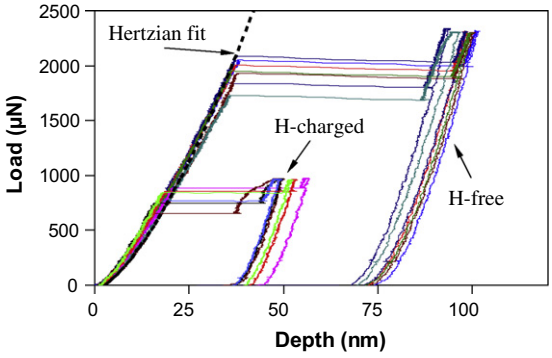

Fig. 7. Typical *L–D* curves of Fe–3 wt.% Si in: (a) air and (b) the hydrogen-charged condition.

4.4. FeAl intermetallic

The commercial importance of iron aluminides for high temperature structural applications has been well established [32]. Iron aluminides contain two of the most widely available metals, namely Fe and Al. They offer low material costs, conservation of strategic materials and lower density than stainless steels, with excellent oxidation and sulfidation resistance. In spite of all these inherent advantages, the binary iron aluminides suffer from hydrogen embrittlement.

A conical indenter with a cone angle of 90° was used to perform the indentations on FeAl intermetallic alloy with 40 at.% Al. The resulting *L–D* curves in different conditions are given in Fig. 8.

4.5. Nickel

The freshly electropolished nickel has a thin (0.6–0.8 nm) film of NiO which can be reduced by cathodic polarization in Na_2SO_4 solution with a pH lower than 8 [33]. Anodic polarization of nickel in the same solution produces a new passive layer, which is a 0.9–1.2 nm film of NiO. This film cannot be reduced in a neutral solution. This fact was used during in situ ECNI experiments to exclude surface effects from the effects of hydrogen [34].

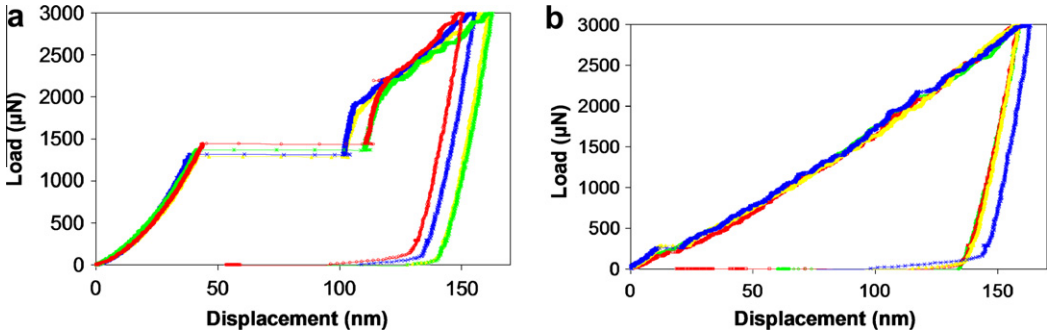

Fig. 8. Typical L–D curves of FeAl in: (a) hydrogen-free and (b) hydrogen-charged conditions.

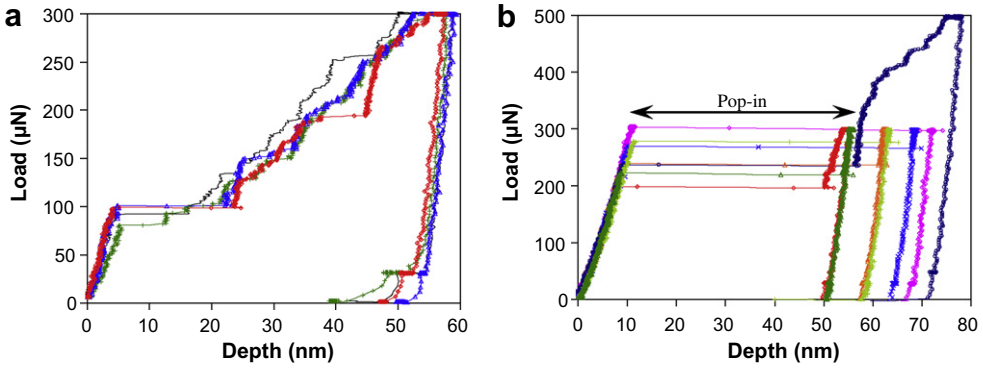

Fig. 9. L–D curves for nickel in: (a) hydrogen-charged and (b) hydrogen-free conditions.

Typical load displacement curves obtained in different condition are shown in Fig. 9.

5. Discussion

The L–D curves of Figs. 5–9 all show three stages: elastic loading, an excursion in depth (pop-in) at the onset of plasticity and continued elastoplastic loading. The initial elastic portion of the loading curves can be fitted with the Hertzian elastic response

$$P = \frac{4}{3} E_r \sqrt{R h^3} \tag{3}$$

where P is the applied load, h is the indentation depth, R is the radius of the tip curvature and E_r is the reduced modulus, given by

$$\frac{1}{E_r} = \frac{1 - v_1^2}{E_1} + \frac{1 - v_2^2}{E_2} \tag{4}$$

Here E is the elastic modulus of the material, v is the Poisson's ratio, and the subscripts 1 and 2 refer to the tip and the sample respectively. The initial elastic loading begins as soon as the tip contacts the material surface and continues until dislocation nucleation or motion occurs. Typical dislocation densities in an annealed metal are in the range 10^6–10^8 cm^{-2}, with dislocations spaced between 1 and 10 μm apart. A typical indentation test in the elastic regime probes a lateral region of at most a couple of hundred nanometers to the point where the pop-in is noted. This suggests the volume of material sampled by the indentation test at this depth is smaller than the average dislocation spacing, so that an indentation placed randomly on the surface would have a significant probability of sampling a region that contains no pre-existing dislocations. Experimental studies [35,36] have been conducted and all lend credibility to the assumption that, for a well-annealed and electropolished sample, the indenter tip can initially contact a volume of material small enough to be dislocation free. The absence of dislocations means the material continues to load elastically until the shear stress under the tip reaches a value near the theoretical shear strength of the material, well above that necessary to activate an existing dislocation source. At this point dislocations are homogeneously nucleated, followed by subsequent glide and multiplication events. Homogeneous dislocation nucleation (HDN) should occur when the stress beneath the indenter tip approaches the theoretical shear strength of the material. The term HDN is used here to indicate that dislocations are nucleated from otherwise dislocation-free material. For an indentation test, the applied shear stress that nucleates a dislocation can be assumed to be the maximum shear stress beneath the indenter during purely elastic loading. According to continuum mechanics, the maximum shear stress is acting on a point 0.48 times the contact radius, a, below the sample surface. Computer simulations have also shown that dislocations nucleate at this point [37]. The position of this maximum shear stress $z_{\tau(\max)}$ and its value $\tau_{\max}$ is given by

Table 5
Summary of the mean pop-in load for the H-charged and H-free conditions and comparison between theoretical strength, $\mu/20$ and measured shear stress at the onset of the pop-in.

Material	Mean $F_{pop\text{-}in}$ (μN)		τ_{max} (GPa)		$z_{\tau(max)}$ (nm)		V (99.9% τ_{max}) (nm^3)		$\mu/20$ (GPa)	R (μm)
	H-free	H-charged	H-free	H-charged	H-free	H-charged	H-free	H-charged		
Copper	380	360	1.23	1.21	95	93	3604	3381	2	3.8
Aluminum	280	80	0.93	0.6	100	65	4203	1154	1.1	3
Fe–3 wt.% Si	2000	840	4.9	3.6	122	82	7633	2318	4.2	2
FeAl	1300	280	5.4	3.2	77	46	1919	409	4.7	1.5
Nickel	185	95	3.3	2.7	37	27	213	83	4	1

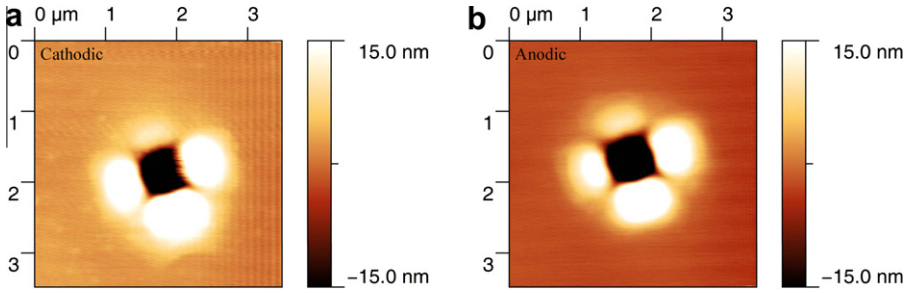

Fig. 10. Surface topography of FeAl sample under: (a) cathodic and (b) anodic potential where no surface roughening was observed.

$$z_{\tau(\max)} = 0.48 \cdot a = 0.48\left(\frac{3PR}{4E_r}\right)^{\frac{1}{3}} \tag{5}$$

$$\tau_{\max} = 0.31\left(\frac{6E_r^2}{\pi^3 R^2}P\right)^{\frac{1}{3}} \tag{6}$$

Table 5 summarizes the effect of hydrogen charging on the mean value of pop-in load τ_{max} and its position below the surface of all studied samples. For comparison, the theoretical strength ($\tau_{th} \approx \mu/20$) according to Frenkel's model is also given in the Table 5.

5.1. Hydrogen effect on HDN

The above results clearly indicate that the pop-in load in the hydrogen-charged condition is lower than in the hydrogen-free condition. This change cannot be attributed to the surface topography since it has been imaged and revealed no surface roughening [24,25]. Fig. 10, as an example, shows the surface topography of the FeAl sample inside the electrolyte. Therefore, the reduction in the pop-in load clearly shows the hydrogen effect on HDN. This is in good agreement with molecular dynamic simulations performed by Wen et al. [37]. Their results, like other experimental NI results on hydrogen-charged materials [18–20], used hydrogen-enhanced plasticity (HELP) to explain the reduction in the pop-in load. However, the analytical description of the HELP mechanism is based on reduction of elastic interactions by solute hydrogen between dislocations and elastic centers which act as barriers, such as nearby dislocations and solute pinning points [12]. As mentioned before, during NI, the probed volume of the material is so small that it can be assumed to be a perfect crystal without any defects. Therefore, elastic shielding of the dislocations by trapped hydrogen atoms is not capable of explaining the observed enhanced plasticity. In adsorption-induced dislocation emission (AIDE) [2,38] the formation energy of dislocations at the crack tip is reduced by hydrogen being absorbed on the crack surfaces. As opposed to HELP, it is the external hydrogen on the crack surface and not the internal hydrogen in the bulk that enhances the dislocation nucleation in AIDE. Therefore, neither HELP (in the original formulation [12]) nor AIDE is capable of explaining the hydrogen-induced reduction in the pop-in load during NI.

According to the classic dislocation theory, the free energy required for HDN during NI is determined by the line energy of the newly formed loop γ_{dis} and the work for extending the dislocation loop τb per loop area. Here τ is the maximum shear stress under the indenter induced by the external load and b is the Burgers vector of the dislocation. If the dislocation forms as a partial, the stacking fault energy (SFE) γ also contributes to the required energy for HDN. Then the formation energy of a circular loop of radius r is

$$\Delta G = 2\pi r\gamma_{dis} + \pi r^2\gamma - \pi r^2 b\tau \tag{7}$$

The elastic self-energy for a full circular dislocation loop of radius r in an infinite elastic solid is given by

$$\gamma_{dis} = \frac{2-\upsilon}{1-\upsilon}\frac{\mu b^2 r}{4}\left(\ln\frac{4r}{\rho} - 2\right) \tag{8}$$

Fig. 11 shows the plots of ΔG as a function of loop radius calculated for the observed mean values of τ_{max} in the hydrogen-charged and hydrogen-free conditions. The material constants used are given in Tables 5 and 6. The free-energy curves for HDN pass through a maximum

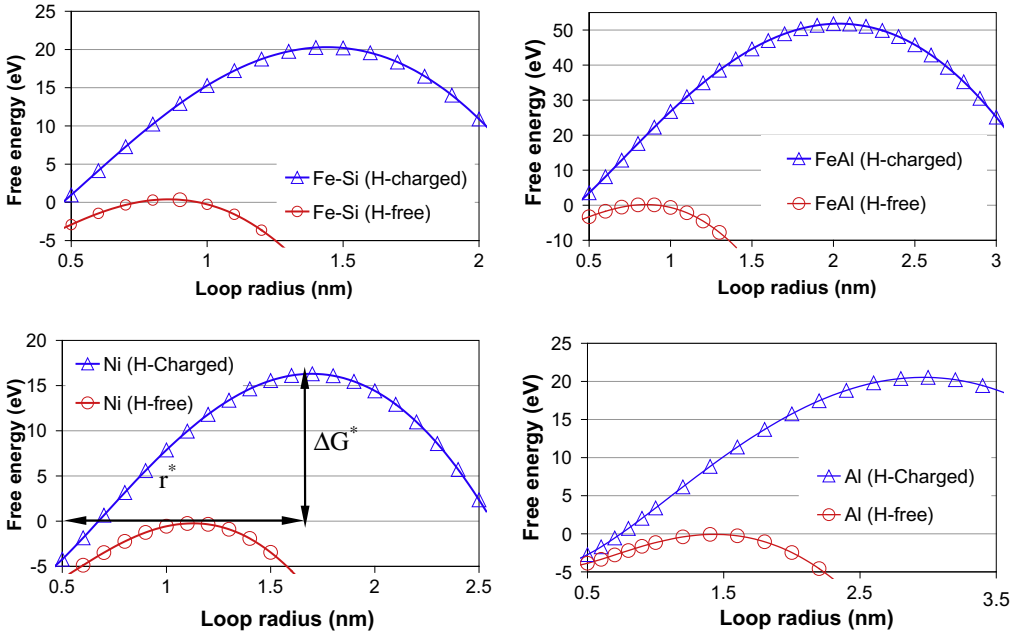

Fig. 11. Free energy curves for examined materials. The activation energy for homogeneous dislocation nucleation, ΔG^*, is the maximum of the free-energy curve at critical loop radius r^*. In the hydrogen-charged condition ΔG^* is too high to overcome by thermal fluctuation available at room temperature.

Table 6
Material constants used to calculate free-energy curves of homogeneous dislocation nucleation.

Material	E_r (GPa)	μ (GPa)	ν	γ (J/m^2)	b (nm)	ρ (nm)	$F_{\text{pop-in(calc)}}$(μN)
Nickel	191	79	0.31	0.24	0.14	0.24	210
Copper	111	42	0.32	0.06	0.15	0.29	377
Aluminum	67	23	0.35	0.17	0.29	0.29	274
Fe–3 wt.% Si	202	85	0.32	0	0.25	0.17	2042
FeAl	217	94	0.3	0	0.25	0.17	1314

which defines the activation energy for HDN (ΔG^*). The ΔG^* at a loop size r^* can be found by setting $\partial \Delta G/\partial r = 0$. In the hydrogen-free condition the free-energy curve for each sample has a maximum of about 0 eV. This means that the process of HDN for the hydrogen-free condition happens spontaneously and without any thermal contribution from the surroundings. Calculated values of pop-in load, $F_{\text{pop-in(calc)}}$ when $\Delta G = 0$ and $\Delta G^* = 0$ are given in Table 6 for comparison. In contrast, the free-energy curves for the hydrogen-charged condition show a relatively high activation energy which must be overcome in order to nucleate a dislocation. Since the tests were performed under the same conditions, there is no possible external contribution for overcoming the activation energy of HDN. The only possible explanation is a reduction in the activation energy for HDN by hydrogen.

Fig. 12 shows the change in the activation energy for HDN due to hydrogen ($\delta \Delta G_H^*$), where good agreement between the known sensitivity of the tested materials and $\delta \Delta G_H^*$ is observed. This is a potential use of ECNI as a technique to evaluate the hydrogen embrittlement sensitivity in extremely small samples for the development of new alloys.

Next, in order to have a better understanding of the effect of hydrogen on HDN, Eq. (7) can be rewritten by introducing the effect of hydrogen as follows:

$$\Delta G = \frac{2-\upsilon}{1-\upsilon}\frac{\mu_H b^2 r}{4}\left(\ln\frac{4r}{\rho_H} - 2\right) + \pi r^2 \gamma_H - \pi r^2 b\tau \qquad (9)$$

where μ_H is the shear modulus under the effect of hydrogen, ρ_H is the hydrogen-affected dislocation core radius and γ_H is the SFE of a hydrogen-containing lattice. The effect of hydrogen on the other parameters involved in Eq. (9) is either negligible or inapplicable. The experimental data can now be used to calculate the effect of hydrogen on μ, γ and ρ. To do this, the rule of spontaneous HDN shall be applied to Eq. (6), i.e. $\Delta G^* = 0$ and $\Delta G = 0$. This results in the following equation:

$$\tau_H = \frac{2-\upsilon}{1-\upsilon}\frac{\mu_H b}{4r^*\pi}\left(\ln\frac{4r^*}{\rho_H} - 2\right) + \frac{\gamma_H}{b} \qquad (10)$$

where τ_H is the shear stress required for the HDN in a hydrogen-charged condition. Eq. (10) shows that the reduction of shear stress required for HDN in a hydrogen-charged sample can be attributed to a decrease in μ_H

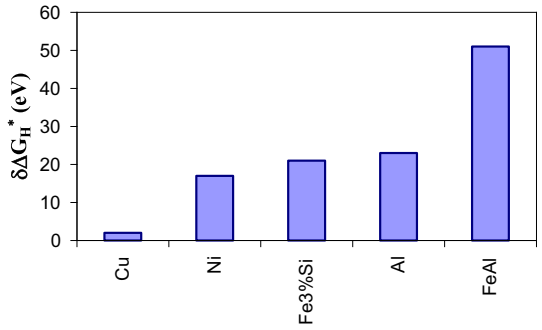

Fig. 12. Change in the activation energy for homogeneous dislocation nucleation by H for tested materials.

Table 7
Summary of the effect of hydrogen on μ, ρ and γ in the samples studied.

Material	Nickel	Copper	Aluminum	Fe–3 wt.% Si	FeAl
$\delta\Delta G_H^*$(eV)	17	2	23	21	51
μ_H (GPa)	50	41	15	62	56
$\Delta\mu/\mu$ (%)	36	2.5	35	27	41
ρ_H (nm)	0.29	0.3	0.41	0.22	0.24
$\Delta\rho/\rho$ (%)	23	2.4	43	37	45
γ_H (J m^{-2})	0.168	0.06	n.a	n.a	n.a
$\Delta\gamma/\gamma$ (%)	24	–	n.a	n.a	n.a

and γ_H, and/or an increase in ρ_H. Table 7 summarizes the effect of hydrogen on μ, γ or ρ for the tested materials when assuming that the hydrogen will affect only one of these parameters.

A source of uncertainty in the present calculations is the fact that a continuum-based description of a dislocation with isotropic properties is used while the problem must ultimately be solved at the atomic level. Furthermore, the exact value of the dislocation core radius is not available. A reasonably exact treatment of HDN with minimal commitment to atomic details using a variational boundary integral method in the Peierls–Nabarro framework has been given recently by Xu and Argon [39]. Within this framework, once the interfacial "constitutive" relation is specified (it could be as simple as the Frenkel sinusoidal law), there is no need for the core cut-off parameter. We compared the Xu and Argon [39] and continuum model results for the HDN activation energy given by Eqs. (7) and (8). Good agreement was found between their results and ours at shear stresses higher than $0.75\tau_{th}$ by setting $\rho \approx b$. Moreover, the difference observed between the hydrogen-charged and hydrogen-free conditions is independent of the dislocation model.

5.2. Hydrogen effect on shear modulus

There are a few reports of experimentally measured changes in elastic properties which are limited to metals with a very high solubility for hydrogen, like palladium [40]. This is essentially because measurements of elastic properties are made on the samples in thermodynamic equilibrium with hydrogen, and it is well known that the equilibrium hydrogen solubility in most metals is very low. On the other hand, hydrogen embrittlement is mainly coupled with local hydrogen enrichment well above the equilibrium solubility. A recent molecular static simulation done by Taketomi et al. [41] shows a 10% reduction in shear modulus by 1 at.% hydrogen dissolved in Fe, which is in very good agreement with the experimental results of Lunarska et al. [42]. Wen's molecular dynamic simulation [43] also shows a 7% reduction in the shear modulus of Ni containing 5 at.% hydrogen. Additionally, Matsumoto et al. [44] used density functional theory and interatomic potential to clearly show that shear strain in body-centered cubic Fe yields a strong hydrogen trap energy, comparable to that of volumetric strain. According to the Hertzian contact model, it is possible to calculate the maximum shear stress under the tip and then numerically estimate the radius of the region where 99.9% of the maximum shear stress is acting [45]. This results in a volume resembling an oblate spheroid formed by rotation of the semi-elliptical part shown in Fig. 13 about its minor axis. The semi-elliptical region has a major axis of $\sim 0.068a$ and a minor axis of $\sim 0.024a$, where $a = 2 \cdot z_{\tau(\max)}$ is the contact radius. This shows that a local reduction in the shear modulus by enrichment of hydrogen in a strained lattice within a very small volume (see Table 5) of the material is enough to reduce the activation energy for dislocation nucleation.

Rose et al. [46] have shown that metallic binding-energy distance curves can be approximately scaled into a single universal relation. Because of this universality, the reduction in the shear modulus is equal to the reduction in the strength of the interatomic bonds, as assumed in the HEDE model. Considering the maximum reductions in μ

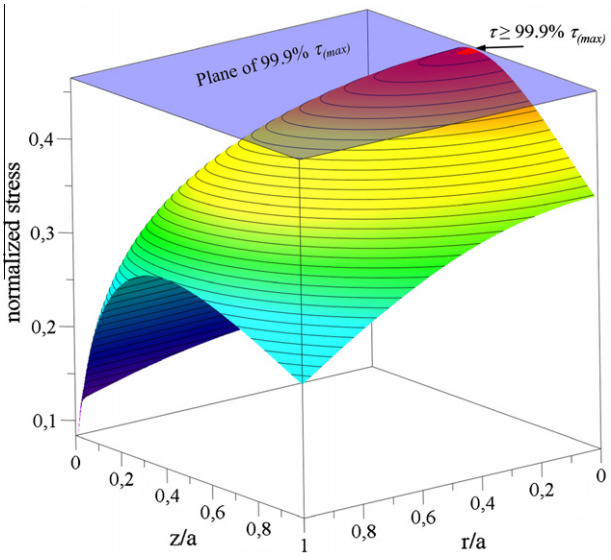

Fig. 13. Shear stress distribution underneath a spherical tip according to Hertz–Huber model. The plane surface defines 99.9% of τ_{max}. The region above this plane defines the volume of material below the tip where is higher than 99.9% of τ_{max}.

by hydrogen as reported by Taketomi et al. [41] for iron (10%) and Wen [43] for nickel (7%), only the reduction in the μ given in Table 7 cannot explain the hydrogen-induced reduction in activation energy for HDN. Furthermore, the magnitude of the reduction in the interatomic bond strength is not sufficient to explain hydrogen embrittlement according to the HEDE mechanism in its original form, as suggested by Troiano [47].

5.3. Hydrogen effect on dislocation core radius and SFE

The Gibbs isotherm is used to define the reduction in the surface energy, γ_S, by segregation of a solute on a surface:

$$d\gamma_S = -\Gamma_A d\mu_A \quad \text{or} \quad \left.\frac{\partial \gamma_S}{\partial \mu_A}\right|_{n_B,T,a} = -\Gamma_A \tag{11}$$

where μ_A is the chemical potential of solute A being segregated with an excess Γ_A at the surface of an area a in a material B of n_B atoms or molecules. Recently it has been proven that Eq. (11) can also be applied to other crystalline defects, like vacancies, dislocations and stacking faults [48]. A new term "defactants (DEFect ACTing AgeNTS)" was introduced [49] in order to cover the action of atoms segregating to defects in solids and reducing their formation energy in the way that surfactants reduce surface energies in liquids. If surfaces and interfaces in solids and liquids are considered to be defects of the continuum, surfactants are a subgroup of defactants. The quantity γ_S in Eq. (11) is now more generally defined as the defect formation energy γ_{defect} and Γ_A has the meaning of an excess solute A per defect dimension Γ_A^{defect}, i.e. excess per vacancy number, excess per dislocation length or excess per stacking fault area [48–50]. Generally, the excess solute at a defect is explained by solute atoms finding sites of lower potential energy at the defect; consequently the solute energy is reduced but not the defect energy (site energy concept). Alternatively, this interaction can be described by assigning the decrease in the overall free energy to a decrease in the defect formation energy (defactant concept). The site energy concept and the defactant concept correspond to different approaches to describing solute/defect interactions. Thus the lowering of the free energy by a reaction of a defect with a solute leading to a defect–solute complex (i.e. excess solute at the defect) may be assigned to either the solute or the defect [49].

Classic dislocation theory relates a reduction in the dislocation line energy γ_{dis} as given in Eq. (8) to an increase in the dislocation core radius or cut-off radius. According to Eq. (11), the solute excess definition for a dislocation, Γ^{dis}, can explain the reduction in γ_{dis} due to defactants (solute hydrogen) in the lattice:

$$\left.\frac{\partial \gamma_{dis}}{\partial \mu_H}\right|_{n,T,V,l_{dis}} = -\Gamma_H^{dis} \tag{12}$$

where μ_H is the chemical potential of the hydrogen atoms dissolved in material with constant number n. The dislocation length l_{dis}, temperature T and volume V are all kept constant. Trapping of hydrogen at dislocations experimentally [50–52] as well as through numerical simulation has been proved [41,53–57].

Reduction of the stacking fault energy by hydrogen has also been reported in several experimental [58–60] and simulation works [41,56,61,62]. In a similar manner, the solute excess definition for a stacking fault Γ^{SF} can be used to derive the change in the Helmholtz free energy per unit area of a stacking fault γ_{SF} by defactants for a constant area of stacking fault, S_{SF}:

$$\left.\frac{\partial \gamma_{SF}}{\partial c_H}\right|_{n,T,V,S_{SF}} = -\Gamma_A^{SF} \tag{13}$$

According to Eqs. (12) and (13), the line energy of a dislocation and the SFE decrease with increasing solute chemical potential if the excess is positive, i.e. solute atoms segregate at the defect. By definition, excess defactant given by Eqs. (12) and (13) is positive and therefore defactants reduce the defect energy.

6. Conclusion

The experimental approaches utilized to locally examine hydrogen embrittlement have been discussed and the fine-scale mechanical probing capability of NI was used to examine hydrogen's effect on HDN. It was shown that hydrogen reduces the pop-in load, which can be attributed to the HELP mechanism. Classical dislocation theory was used to model HDN and it was shown that hydrogen reduces the activation energy for HDN ($\delta\Delta G_H^*$). The change in $\delta\Delta G_H^*$ can be used to rank the sensitivity to hydrogen embrittlement. Of the materials tested, copper shows a very low sensitivity to hydrogen embrittlement and the intermetallic FeAl alloy shows the highest. The activation energy for HDN is related to the material-specific parameters: μ, ρ and γ. These material properties can be influenced by hydrogen, resulting in reduced activation energy for dislocation nucleation.

The universality of cohesive energy in metals relates the reduction in the shear modulus to the reduction in cohesion. This reduction in interatomic binding forces is not enough to support the HEDE mechanism but can only influence the elastic energy of the dislocations. The defactant concept is used to explain the additional reduction in the dislocation line energy within the dislocation core in the presence of hydrogen. In the case of partial dislocations in face-centered cubic crystals, the SFE can also be reduced by hydrogen according to the defactant model.

Thus, the process of hydrogen embrittlement is controlled by a decrease in the defect formation energy and a reduction in the interatomic bonding energy. Depending on the experimental approach utilized to study hydrogen embrittlement, the results can be interpreted as HELP or HEDE. By utilizing an appropriate experimental approach, it was possible to show that neither HEDE nor HELP in

their original form are able to explain hydrogen embrittlement on the nanoscale. In contrast, the defactant concept and decohesion can successfully describe the hydrogen embrittlement. The suggested approach is being used to study hydrogen embrittlement in industrially important alloys with complex microstructures and compositions, and will be the topic of a future publication.

Acknowledgements

This work was sponsored by DFG under contract VE 132/25-1. The authors would like to thank Prof. E.P. George from Oak Ridge National Lab for providing FeAl single crystals. The authors are grateful for the helpful discussion with Mao Wen, AIST, Japan, and are grateful to Jules Dake for proofreading.

References

[1] Johnson WH. Proc Roy Soc London 1875;23:168.
[2] Lynch S. In: International conference on hydrogen effects on materials behavior and corrosion deformation interactions, Moran, WY, USA; 2002. p. 449–66.
[3] Gangloff RP. Critical issues in hydrogen assisted cracking of structural alloys. Oxford: Elsevier Science; 2005.
[4] Pundt A, Kirchheim R. Annu Rev Mater Res 2006;36(1):555.
[5] Borchers C, Michler T, Pundt A. Adv Eng Mater 2008;10:11.
[6] Tkachov VI, Vytvyts' kyi VI, Berezhnyts' ka MP, Ivas' kevych LM. Mater Sci 2008;44(4):561.
[7] Olden V, Thaulow C, Johnsen R, Østby E, Berstad T. Eng Fract Mech 2009;76(7):827.
[8] Zmudzinski C, Pressouyre G, Bretin L. Commission of the European Communities (first programme on the production and utilization of hydrogen); 1982.
[9] Vehoff H, Neumann P. Acta Metall 1980;28:265.
[10] Vehoff H, Rothe W. Acta Metall 1983;31:1781.
[11] Vehoff H, Klameth HK. Acta Metall 1985;33(6):955.
[12] Birnbaum HK, Sofronis P. Mater Sci Eng A 1994;A176(1–2):191.
[13] Bond GM, Robertson IM, Birnbaum HK. Scr Metall 1986;20(5):653.
[14] Golovin Y. Phys Solid State 2008;50(12):2205.
[15] Katz Y, Tymiak N, Gerberich WW. Eng Fract Mech 2001;68:619.
[16] Glowacka A, Wozniak M, Swiatnicki W. Rev Adv Mater Sci 2004;8(1):66.
[17] Gao X. Scr Mater 2005;53:1315.
[18] Zhang L, An B, Fukuyama S, Yokogawa K. Jpn J Appl Phys 2009;48(8):08JB08.
[19] Bahr D, Nibur K, Morasch K, Field D. JOM 2003;55(2):47.
[20] Nibur KA, Bahr DF, Somerday BP. Acta Mater 2006;54:2677.
[21] Durst K, Backes B, Franke O, Göken M. Acta Mater 2006;54:2547.
[22] Vehoff H, Yang B, Barnoush A, Natter H, Hempelmann R. Z Phys Chem 2008;222:499.
[23] Welsch MT, Henning M, Marx M, Vehoff H. Adv Eng Mater 2007;9:31.
[24] Barnoush A, Bies C, Vehoff H. J Mater Res 2009;24(3):1105.
[25] Barnoush A, Vehoff H. Corros Sci 2008;50:259.
[26] Barnoush A, Vehoff H. Scr Mater 2006;55:195.
[27] DeWulf DW, Bard AJ. J Electrochem Soc 1985;132:2965.
[28] Nisancioglu K, Holtan H. Corros Sci 1979;19(8):537.
[29] Barnoush A, Vehoff H. Scr Mater 2008;58:747.
[30] Stumm W. Chemistry of the solid–water interface. New York: Wiley; 1992.
[31] McCafferty E. J Electrochem Soc 2003;150:B342.
[32] Palm M. Int J Mater Res 2009;100(3):277.
[33] Scherer J, Ocko BM, Magnussen OM. Electrochim Acta 2003;41:1169.
[34] Barnoush A, Vehoff H. Int J Mater Res 2006;97:1224.
[35] Barnoush A, Yang B, Vehoff H. Effect of hydrogen and grain boundaries on dislocation nucleation and multiplication examined with a NI-AFM, vol. 47. Berlin: Springer; 2008. p. 253.
[36] Vehoff H, Yang B, Barnoush A, Natter H, Hempelmann R. Mechanical properties of nanomaterials examined with a NI-AFM, vol. 2. Oldenbourg: Oldenbourg Wissenschaftsverlag; 2008. p. 275–301.
[37] Wen M, Zhang L, An B, Fukuyama S, Yokogawa K. Phys Rev B 2009;80(9):094113.
[38] Lynch SP. In: Proceedings of the international conference on hydrogen effects on material behaviour and corrosion deformation interactions; 2003. p. 449–66.
[39] Xu G, Argon AS. Mater Sci Eng A 2001;319–321:144.
[40] Farraro RJ, McLellan RB. J Phys Chem Solids 1978;39(7):781.
[41] Taketomi S, Matsumoto R, Miyazaki N. Int J Mech Sci 2010;52(2):334.
[42] Lunarska E, Zielinski A, Smialowski M. Acta Metall 1977;25(3):305.
[43] Wen M. Private communication.
[44] Matsumoto R, Inoue Y, Taketomi S, Miyazaki N. Scr Mater 2009;60(7):555.
[45] Barnoush A. Hydrogen embrittlement, revisited by in situ electrochemical nanoindentation. Herzogenrath: Shaker Verlag GmbH; 2009.
[46] Rose JH, Smith JR, Guinea F, Ferrante. J Phys Rev B 1984;29(6):2963.
[47] Troiano A. Trans ASM 1960;52(1):54.
[48] Kirchheim R. Acta Mater 2007;55(15):5129.
[49] Kirchheim R. Int J Mater Res 2009;100(4):483.
[50] Kirchheim R. Acta Mater 2007;55(15):5139.
[51] Hong GW, Lee JJ. Acta Metall 1984;32:1581.
[52] Maxelon M, Pundt A, Pyckhout-Hintzen W, Kirchheim R. Scr Mater 2001;44(5):817.
[53] Matsumoto R, Taketomi S, Matsumoto S, Miyazaki N. Int J Hydrogen Energy 2009;34(23):9576.
[54] Taketomi S, Matsumoto R, Miyazaki N, Taketomi S, Matsumoto R, Miyazaki N. Acta Mater 2008;56(15):3761.
[55] Chateau JP, Delafosse D, Magnin T. Acta Mater 2002;50:1507.
[56] Wen M, Fukuyama S, Yokogawa K. Scr Mater 2005;52:959.
[57] Wen M, Fukuyama S, Yokogawa K. Acta Mater 2003;51:1767.
[58] Miyata K. Metall Mater Trans A 2003;34A(6):1249.
[59] Hermida J, Roviglione A. Scr Mater 1998;39(8):1145.
[60] Ferreira P, Robertson I, Birnbaum H. Mater Sci Forum 1995;207:93.
[61] Chandler MQ, Horstemeyer MF, Baskes MI, Gullett PM, Wagner GJ, Jelinek B. Acta Mater 2008;56(1):95.
[62] Wen M, Fukuyama S, Yokogawa K. Phys Rev B 2004;69:174108.